Journal of Hydrology 570 (2019) 118–131

Contents lists available at ScienceDirect

Journal of Hydrology

journal homepage: www.elsevier.com/locate/jhydrol

Research papers

Incorporating climate model similarities and hydrologic error models to quantify climate change impacts on future riverine flood risk

Kuk-Hyun Ahn[a,*], Yong-Oh Kim[b]

[a] Department of Civil and Environmental Engineering, KongJu National University, Cheon-an, South Korea
[b] Department of Civil and Environmental Engineering, Seoul National University, Seoul, South Korea

ARTICLE INFO

This manuscript was handled by G. Syme, Editor-in-Chief, with the assistance of Joseph H.A Guillaume, Associate Editor

Keywords:
Quantifying uncertainty
Climate change
Hydrologic response

ABSTRACT

Quantifying uncertainty in projecting climate change impact on flood frequency analysis is particularly relevant for long-term water resources planning and management. This study examines uncertainties arising from (1) a climate model, with and without accounting of intermodel similarities, (2) a hydrological model with two different error model definitions, which have previously received less attention in studies propagating uncertainty through climate change impacts on flood response. Through a Bayesian modeling framework, a proposed statistical framework is utilized to explore various definitions of sources of uncertainty and to develop a series of nested formulations that can evaluate the leverage of specific uncertainty sources in quantiles of future streamflow. To be specific, climate model similarity, hydrologic prediction error, and frequency analysis are formally modeled with an appropriate likelihood function. The quantiles inferred by each formulation are compared in a case study of the Yongdam Basin in Korea. Results indicate that variance in hydrologic response is underestimated if climate model similarities are ignored, and in many cases, the inferred quantiles of streamflow projection are biased accordingly. Furthermore, a simple error model used in defining hydrologic uncertainty may create incorrect information in determining the quantiles in streamflow projection. The approach presented here of quantifying uncertainty has the potential to better depict overall multi-source uncertainties in projections of climate change impacts on hydrologic response. Finally, our results also indicate that careful flood planning management may be required for the Yongdam Basin in future summers.

1. Introduction

The possible impacts of climate change have been increasingly examined to project the long-term needs of local water resources management (Franco et al., 2011; Zhuang et al., 2018). In particular, many studies have shown that flood risk can be significantly affected by climate change (Arnell and Gosling, 2016; Qi et al., 2016). Assessing the impacts of climate change entails a large degree of uncertainty when appraising its projected impact on floods (Chen et al., 2011). In projecting climate change impacts, various sources of uncertainty have been identified and diverse methodologies have been developed to quantify respective contributions (Nguyen et al., 2016; Shen et al., 2018; Zhuang et al., 2018). However, this diversity rather hinders a straightforward evaluation of water resource infrastructure and may lead to misinterpretation of overall uncertainty. Understanding changes in uncertainties corresponding to the formulations of a contribution helps to design climate impact analysis with a more robust uncertainty assessment. This is the primary contribution of this work, by proposing a statistical framework in which the uncertainties are accounted for and propagated through analysis.

Most studies evaluate the frequency of flooding to climate change by relying on future climate scenarios (e.g., simulated by global climate models – GCMs, statistically or dynamically downscaled and/or bias-corrected and fed into hydrological models). The simulated flood response is then compared to a baseline response estimated on historic climate data (e.g., Karlsson et al. (2016); Van Huijgevoort et al. (2014)). In the process, quantifying individual contributions from future climate conditions to flood response is required for full analysis of uncertainty under climate change (Bosshard et al., 2013) so that decision makers can consider adaptation strategies contextualized by the uncertainty in design statistics. Significant research attention has been gained with multiple uncertainty sources, including those related to GCM structure, greenhouse gas emission scenarios (Fang et al., 2015; Ficklin et al., 2016), the choice of downscaling method (Etemadi et al., 2014; Li et al., 2015)), hydrologic modeling (i.e., model structure (Bae et al., 2011; Poulin et al., 2011; Troin et al., 2017), and uncertain

* Corresponding author.
E-mail addresses: ahnkukhyun@gmail.com (K.-H. Ahn), yokim05@snu.ac.kr (Y.-O. Kim).

https://doi.org/10.1016/j.jhydrol.2018.12.061
Received 28 June 2018; Received in revised form 19 December 2018; Accepted 21 December 2018
Available online 11 January 2019
0022-1694/ © 2019 Elsevier B.V. All rights reserved.

parameterization (Brigode et al., 2013; Dobler et al., 2012)), and frequency analysis model (Quintero et al., 2018; Viglione et al., 2013)).

The most common approach to defining climate conditions is developing a multi-model ensemble prediction by considering a number of simulations from a range of different GCMs (Christierson et al., 2012; Hall et al., 2012; Lee et al., 2017; Qi et al., 2016; Xu et al., 2010). This approach generally assumes that each individual climate model is considered as an independent representation of the Earth system, implying that there are not too many similarities that would bias output from each GCM. However, the GCMs are often similarly performed in many cases for various reasons (e.g., coarse resolution (Knutti et al., 2013), calibration data sets (Abramowitz and Bishop, 2015), and shared code components (Pennell and Reichler, 2011)). For instance, climate models that are fundamentally different with respect to certain underlying processes can show similar climate representations if the models have been particularly developed based on the same observational data sets to calibrate and evaluate present-day climate conditions (Abramowitz and Bishop, 2015). Also, if scientists make a number of simplifications in model resolutions, climatic deviations from the models will be similarly performed. In the extreme case, a model run at two resolutions provides very little additional information about averaged climatic projection (Masson and Knutti, 2011). To address this dependence, recent studies have proposed a method to combine the GCMs for the multi-model ensemble predictions applying less weight to GCMs which are similar (Haughton et al., 2015; Sanderson et al., 2015). As presented by Haughton et al. (2015), dependence-based ensemble prediction is substantially beneficial both to long-term planning and uncertainty quantification that are relevant for assessing climate change impact. Although very important, the similarities have received less emphasis in studies investigating uncertainty analysis of hydrologic alteration under climate change.

In addition to the uncertainty in future climate simulations, there is also significant uncertainty surrounding the ability of the hydrologic model. There are many studies exploring the impact of hydrologic model uncertainty on the assessment of climate impact, but they often focus on parameters, structural errors, or a combination of both (Chen et al., 2011; Dobler et al., 2012; Kay et al., 2009; Lee et al., 2017; Poulin et al., 2011; Qi et al., 2016), However, these uncertainties may not provide reliable bounds for streamflow estimates (Steinschneider et al., 2012) because flood responses may be difficult to simulate only with an ensemble of model structures or parameterization, considering that the hydrological processes in most watersheds are known to exhibit highly nonlinear behavior (Sivakumar and Singh, 2012). Renard et al. (2011) also concluded that predictive error models improve the reliability of the integrated uncertainty estimates in hydrologic modeling. To generate reliable predictive bounds of flood estimates, formal quantification of predicted errors inherent in a hydrologic model is needed through climate change impact analyses.

The predictive error model is generally built based on a statistical description of the differences between the model predictions and observed data. Properly characterizing the form of the errors is required to provide reliable and precise hydrologic predictions (Smith et al., 2010). If an inadequate model is used for the properties of predictive errors, unreliable parameter estimates and inadequate predictions are obtained (Evin et al., 2014). It is particularly important when hydrologic models are applied in forecasting periods similar to climate change impact analyses (Zhang et al., 2008). Because of the benefits of explicitly stated assumptions, it is often the case that the predictive errors are independent and identically distributed (i.e., iid) according to a normal distribution with mean zero and a constant variance (e.g., Sun and Bertrand-Krajewski, 2013; Zhang et al., 2016). However, this simple assumption has been criticized by its many applications (Beven et al., 2008).

In many hydrological applications, the errors are autocorrelated, nonstationary, and non-normal (Sun et al., 2017). A common form of nonstationarity is heteroscedasticity, especially in the form of an increase in error variance with streamflow discharge. Recent studies have proposed methodologies to deal with these features in a hydrologic model (Evin et al., 2014; Honti et al., 2013; McInerney et al., 2017). In particular, Schoups and Vrugt (2010) model the prediction errors by using the first order autocorrelation (AR1) process, a time-variant function linearly related with predicted flow, and a random noise component described by a skew exponential power distribution. These flexible parameterizations allow the structure of prediction errors to capture the salient features in the errors, which have received less attention in studies propagating uncertainty through climate impact assessments of hydrologic alteration. To the authors' knowledge, few studies have attempted to simultaneously propagate uncertainty using the errors' features (Zhang et al., 2016). Zhang et al. (2016) employed a Bayesian framework to evaluate uncertainty in parameters for the impact of climate change on streamflow. In that study, AR1-transformed prediction errors have been employed despite the errors in a hydrologic model exhibiting more complex features.

This study presents a Bayesian framework in which climate model similarity and hydrologic error uncertainty are formally characterized and examined to better quantify the integrated propagated uncertainty of hydrologic alterations under future climates. This framework allows a comparison of the range of projected changes in streamflow with several variants of modeling formulations to test specific uncertainty considerations, highlighting the complex interactions between variously defined sources of uncertainty and their effects on future estimates of design flow statistics used in decision making. Climate model similarity and hydrologic prediction error are formally structured with an appropriate likelihood function and combined with priors of model parameters using Bayes' theorem. Then, uncertainty bounds, expressed as the variability of the design value under consideration, are extended for assessment of their impact on climate change. Summing up, we seek to answer the following questions in a case study of daily streamflow in the Yongdam Basin located in South Korea by utilizing the proposed uncertainty assessment framework:

1. How can projected probabilistic changes in streamflow differ with and without accounting for intermodel correlations in climate models?
2. How can projected probabilistic changes in streamflow be affected by the formulation of predictive error models in a hydrologic model?
3. What probabilistic changes in future streamflow are expected if climate model similarity and a probabilistic error model are considered simultaneously when they are compared with historical streamflow?

The remainder of this paper is organized as follows. The data and study area are described in Section 2. Section 3 presents a statistical framework for quantifying the integrated uncertainty of hydrologic alteration under the effects of climate model similarity and hydrologic uncertainty. The proposed framework is applied and the propagated uncertainties presented in Section 4. Finally, the paper concludes in Section 5 with a discussion of the limitations of our approach and future research needs.

2. Study areas and data

The Geum River Basin drains the Geum River estuary into the Yellow Sea and is located in Midwest Korea with a drainage area of about 9810 km^2 (Jeong et al., 2014). Because the basin is located in a transitional zone with climate influenced by northeastern Asia and the western Pacific Ocean, climate in winters is influenced mainly by the Siberian High, whereas summers are affected by hot and humid conditions generated by the Maritime Pacific High (Vieux et al., 2009). Transitional seasons between winter and summer are generally dry, which periodically bring droughts. Interannual precipitation is rather

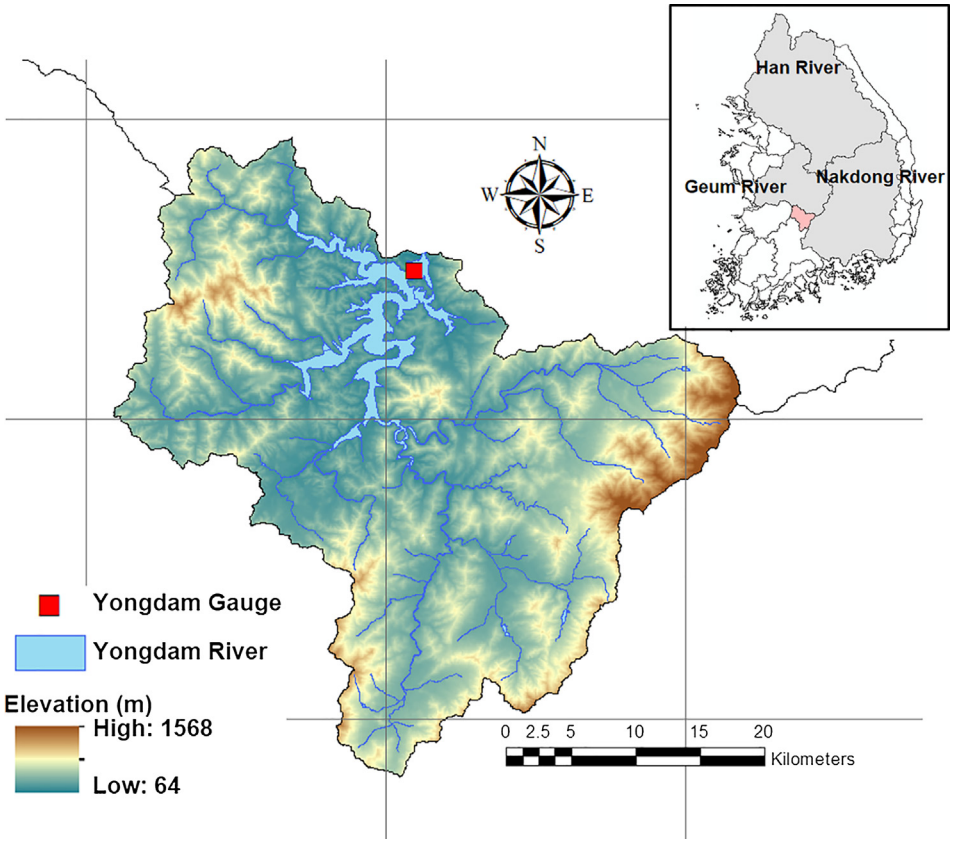

Fig. 1. Map of the Yongdam watershed. The grid points of the climate models (1/2 degree resolution) are presented. Inset: the location (red color) of our study area in the Korean peninsula is presented. (For interpretation of the references to color in this figure legend, the reader is referred to the web version of this article.)

variable. In the last 50 years, average annual precipitation has been 1290 mm with high and low of 1783 mm and 754 mm, respectively. Approximately two-thirds of annual precipitation is concentrated in the summer spanning from late June to early September while precipitation in winter represents less than 10% of annual precipitation. Summers are also affected by the generation of extraordinarily high rainfall and corresponding floods by monsoonal moisture that encroaches on the Korean Peninsula from the intertropical convergence zone (Yan et al., 2015).

In addition to the complexity of regional climate systems, the basin has also faced many water-related issues, including water quality control, fish flow requirements, eutrophication from rising water temperatures, and drastically increased water demand due to regional population growth (Ryu et al., 2011). Over the last decade, the region has experienced several severe droughts resulting in decreased availability of water resource (Seo et al., 2018). These challenges highlight the need to build better adaptive water resources management plans integrating an uncertain future climate.

To analyze hydrologic alteration within climate change, we selected the Yongdam Basin, one of the sub-basins in the Geum River Basin (Fig. 1). While most parts of the Geum River Basin are regulated by reservoirs, the Yongdam Basin located upstream is relatively free from artificial diversions and human adjustments. The Basin draining northward to the Yongdam multipurpose dam is characterized by steep mountain terrain with flat-gradient river networks, particularly in the lower reaches. The terrain slope is moderately steep, averaging 17.6% with a maximum grade of 68%, and a minimum channel slope of 0.06%.

Historic daily climate data, including precipitation, maximum and minimum temperatures were gathered from 63 of the Korea Meteorological Administration's Automated Surface Observing System (ASOS) gauges. The data was interpolated onto a 1/8 degree resolution ($\sim 140\ km^2$) by using the Thiessen polygons (Thiessen, 1911). The final daily data set was obtained for the period of 1 January 1975 to 31 December 2004 by averaging the values within each grid cell overlapping our study basin area (the location of the grid points are presented in Fig. 1). Daily observed streamflow data were gathered from the Water Resources Management Information System webpage (http://www.wamis.go.kr/) for the period of 1 January 2001 to 31 December 2010. Note that the streamflow data are available only beginning in the year 2001 upon completion of the Yongdam Reservoir.

Finally, three climate variables-monthly precipitation, maximum and minimum temperatures-were gathered from thirty-seven climate models of the World Climate Research Programme's Coupled Model Intercomparison Project Phase5 (CMIP5) multi-model data sets (Taylor et al., 2012) with the Representative Concentration Pathway (RCP) 8.5 and historical scenarios (Meinshausen et al., 2011). Only a single run based on a single set of initial conditions is considered in the analysis. Table S1 presents a list of the GCMs employed in this study. Historical simulations and future projections are developed using 30-year windows, 1971–2000 (baseline) and 2051–2080 (2060 target year), respectively. Chen and Brissette (2017) reported that to eliminate the risk of grid-point numerical effect in climate model outputs, averaging more than a few grid points even in the case of small watersheds is necessary. Accordingly, we first interpolated model outputs bilinearly to a resolution of 1/2 degree and then averaged final outputs from nine grid points near our study basin.

3. Methodology

The methodology to explore how climate model similarity and hydrologic uncertainty influence integrated uncertainty is comprised of four major components. The first modifies the approach of Steinschneider et al. (2015) to consider the effects of climate model

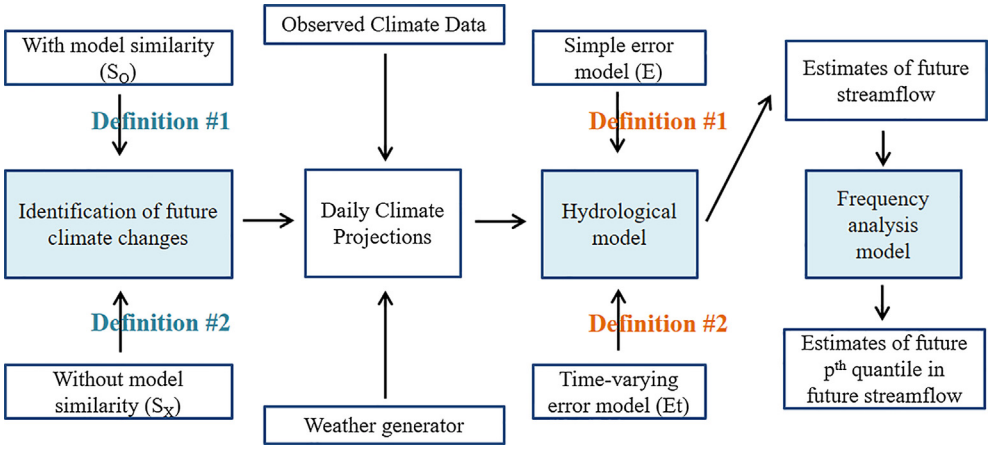

Fig. 2. Flowchart of the statistical framework for identifying uncertainties generated by the different definitions of climate change and hydrologic model. Three uncertainty sources are highlighted.

similarities accommodating changes in climate variables (Section 3.1). The second component utilizes the method of Evin et al. (2014) to characterize parametric and predictive uncertainty using a Bayesian calibration framework (Section 3.2). The third component presents a frequency analysis theory to estimate values of the given probabilities for a flow time series (Section 3.3). Section 3.4 presents the overall framework proposed to propagate uncertainty of each contribution. The framework is briefly presented in Fig. 2 and a detailed description of each step is further provided in the following sections.

3.1. Future climate projections

3.1.1. Probability model for climate change

In accordance with Knutti et al. (2013), we define model similarity as similarity in the model outputs. To account for the similarity of climate models, probability distributions for changes in midcentury minimum and maximum temperatures and precipitation are estimated in a Bayesian framework through Eq. (1):

$$C^A \; N(\mu^A, \Sigma^A) \tag{1.1}$$

$$C^M \; N(\mu^M + \tau^M(C^A - \mu^A), \Sigma^M) \tag{1.2}$$

$$C^P \; N(\mu^P + \tau^P(C^A + C^M - \mu^A - \mu^M), \Sigma^P) \tag{1.3}$$

$$C^A \; N(\mu^A + \beta^A(C^A - \mu^A), \theta^A\Sigma^A) \tag{1.4}$$

$$C^M \; N(\mu^M + \beta^M(C^M - \mu^M) + \tau^M(C^M - \mu^M), \theta^M\Sigma^M) \tag{1.5}$$

$$C^P \; N(\mu^P + \beta^A(C^A - \mu^A) + \beta^M(C^M - \mu^M) + \tau^P(C^A + C^M - \mu^A - \mu^M), \theta^P\Sigma^P) \tag{1.6}$$

where, C^A, C^M, and C^P are the vectors of historical monthly minimum and maximum temperatures and precipitation, respectively, simulated by climate models. Similarly, C^A, C^M, and C^P are the vectors of future monthly minimum and maximum temperatures and precipitation, respectively. The historical means (μ^A, μ^M, and μ^P) and future means (μ^A, μ^M, and μ^P) are assumed to be the true mean values represented by the climate models. Changes of interest are quantified by the difference between expected future and historical outputs (i.e., $N(\mu,\theta\Sigma) - N(\mu, \Sigma)$) developed with 800 random samples. The coefficients τ capture linear correlations between two covariates whereas the coefficients β link historical and future simulations. The covariance matrices are designed to account for model similarities and allow covariance to vary from the historical (Σ) to the future matrix (Σ). The diagonal terms in both matrices are identical ($\lambda_{i,i}$). The off-diagonal terms capture the historical and future correlation between climate models, $\rho_{i,\hat{i}}$ and $\rho_{i,\hat{i}}$, respectively. For example, the ith and $\hat{i}$th off-diagonal terms for the historical and future covariance matrices are set to be $\rho_{i,\hat{i}}\lambda_i^{\frac{1}{2}}\lambda_{\hat{i}}^{\frac{1}{2}}$ and $\rho_{i,\hat{i}}\lambda_i^{\frac{1}{2}}\lambda_{\hat{i}}^{\frac{1}{2}}$ respectively. The coefficients θ then capture changes in the historical and future variance parameters. Note that we utilize the individualized correlations in historical (future) scenarios for all models whereas Steinschneider et al. (2015) design the correlations to be constant across the same model family members, e.g. the single correlation is provided for all the CCSM/CESM models within the National Center for Atmospheric Research (NCAR).

The Bayesian framework is applied independently for each of the twelve months separately and is coded for full Bayesian inference using the slice sampler in the JAGS programming language (Plummer, 2003). Two chains are run with overdispersed initial values for posterior exploration. After running 10,000 burn-in simulations, the posterior distributions are defined with 8000 iterations, thinned to every twentieth draw to reduce sampling dependence. Convergence is evaluated based on chain mixing using a Gelman and Rubin convergence threshold of 1.1 (Gelman et al., 2014). All parameters are estimated with vague prior distributions whereas intermodel correlations are calculated in data from a defined period (described in Section 2).

If no correlation structures between the climate models are used, historical and future simulations in climate models are assumed to follow univariate Gaussian distributions, with correlations and hence off-diagonals set to zero and each variance parameter estimated independently. This approach is quite comparable to the concept of those used for the purpose of uncertainty analysis of hydrologic alteration under climate change (Christierson et al., 2012; Hall et al., 2012; Lee et al., 2017; Qi et al., 2016) although they do the inference for each model separately without creating an explicit matrix structure. We employ the "matrix structure" approach to evaluate the effects of model similarity in this study.

3.1.2. Daily climate scenarios generation

To generate an ensemble of daily climate scenarios with changes ($N(\mu,\theta\Sigma) - N(\mu, \Sigma)$) estimated by two approaches with or without accounting for intermodel correlations, a weather generator developed by Cordano and Eccel (2016) is employed for precipitation, maximum, and minimum temperatures. The weather generator adopts a vector autoregressive (VAR) model to maintain temporal correlations among generated daily precipitation and temperature data. The auto-regression order must be determined prior to scenario generation and is decided based on the akaike information criterion (AIC) (Eq. (2); Akaike, 1981) calculated from the observed data:

$$\mathrm{AIC} = 2\chi - 2\ln(L) \tag{2}$$

where χ is the number of estimated parameters in the model and L is the likelihood function for the model.

Table 1
Summary of prior distributions for M_{E_t}

	Parameter	Prior distribution	Posterior distribution			
			1st quartile	Median	Mean	3rd quartile
GR4J model	Ω_1	Uniform (1, 1000)	125.7	130.2	130.3	134.9
	Ω_2	Uniform (−2, 2)	1.545	1.589	1.585	1.628
	Ω_3	Uniform (1, 1000)	18.13	18.95	18.93	19.74
	Ω_4	Uniform (0.1, 100)	1.179	1.195	1.196	1.213
Error model	ϑ_0	Uniform (0, 1)	0.128	0.135	0.135	0.141
	ϑ_1	Uniform (0, 1)	0.551	0.559	0.560	0.568
	ζ_1	Uniform (0.1, 10)	0.376	0.412	0.414	0.450
	ζ_2	Uniform (−1, 1)	0.311	0.321	0.322	0.333

A more detailed description of the information about the weather generator can be found in Cordano and Eccel (2016). The simulated scenarios obtained by the weather generator enable us to examine the effects of changes in climate variability because they exhibit identical statistical changes while being independently generated.

3.2. Hydrologic modeling

This study uses a parsimonious daily lumped rainfall-runoff model with quick and slow flow components, the GR4J (Modèle du Génie Rural à 4 paramètres Journalier) model (Perrin et al., 2003), which is a modified version of the GR3J model originally proposed by Edijatno et al. (1999). The GR4J model has a simple structure representing interception, infiltration, and percolation using four parameters (Table 1) and requires two types of inputs: precipitation and potential evapotranspiration (PET) time series. Note that spatial averaging of inputs is used because GR4J is a hydrological lumped model. The GR4J model first calculates net rainfall or evapotranspiration by subtracting PET from precipitation. If there is net rainfall, a portion enters the production store in which the actual evaporation is calculated and percolation occurs. The percolated water reaches the flow routing through leakage. Another portion of precipitation goes directly to the flow routing. The total quantity of water that reaches routing is then split into two flow components: 90% of the water is routed by a unit hydrograph and then a non-linear routing store, and the remaining 10% is routed by a single unit hydrograph. Total streamflow is finally obtained by adding these two parts together. Here, the first parameter (Ω_1) determines the size of the production store, the second parameter (Ω_2) controls the flux to groundwater, the third parameter (Ω_3) manages the size of the routing store, and the last parameter (Ω_4) controls the recession of the unit hydrograph. If there is net evaporation, actual evaporation is calculated based on the level of water in the production store. For more details on GR4J, a more thorough description of the theory can be found in Perrin et al. (2003). This study also uses the Hargreaves method (Hargreaves and Samani, 1982) for estimating PET from maximum and minimum temperatures. Radiation values for the Hargreaves method are estimated by the method proposed by Allen et al. (1998).

To account for autocorrelated, heteroscedastic and non-normal residuals, the error term ε is modified similar to approaches in Steinschneider et al. (2015b). Assume that streamflow Q is modeled as the model (M_{E_t}) estimates $\widehat{Q}(C^P, C^{PET}|\ \Omega)$ and the error term ε (Eq. (3)). Then, the error term is modified using Eqs. (4)–(7).

$$Q_t = \widehat{Q}(C^P, C^{PET}|\ \Omega) + \varepsilon_t \tag{3}$$

$$\delta_t = \frac{\varepsilon_t}{\xi_t} \tag{4}$$

$$\xi_t = \vartheta_0 + \vartheta_1 \widehat{Q_t} \tag{5}$$

$$\varrho_t = \delta_t - \vartheta_2 \delta_{t-1} \tag{6}$$

$$\varrho_t \sim SEP(0, 1, \zeta_1, \zeta_2) \tag{7}$$

where Ω is a parameter set of the hydrologic model, δ_t is a normalized error term, ξ_t is a time-varying standard deviation, ϑ_0 and ϑ_1 are the coefficients of a linear regression as a function of the predicted flow, ϑ_2 is the autoregression coefficient and ϱ_t is assumed to follow a skew exponential power (SEP) distribution with mean 0, standard deviation 1, skew ζ_1 and kurtosis ζ_2, respectively. As applied in Evin et al. (2013), the standard deviation of ϱ_t is set to $\sqrt{1-\vartheta_2}$ in this study.

All parameters of the GR4J model and the error model parameters are calibrated (validated) by using the observed data from January 2001 to December 2008 (January 2009 to December 2010). Here, vague uniform distributions (presented in Table 1) are used in a Bayesian framework to investigate parametric uncertainties. We also calibrate the GR4J model with a normal likelihood function with a mean of 0 and a constant variance σ^2 (M_E) to compare with the error model accounting for autocorrelated, heteroscedastic, and non-normality in hydrologic response. The likelihood functions for M_{E_t} and M_E for the observed streamflow Q can then be computed as follows:

$$L^{M_{E_t}}(Q_{1:T}|\ \Omega, \zeta_1, \zeta_2, C^P, C^{PET}) = \prod_{t=1}^{T} \frac{1}{\xi_t} \times \frac{2\xi_\zeta}{\zeta_1 + \zeta_1^{-1}} \omega_{\zeta_2} \exp\left(-c_{\zeta_2}\ |\alpha_{\zeta_1,t}|^{\frac{2}{(1+\zeta_2)}}\right) \tag{8}$$

$$L^{M_E}(Q_{1:T}|\ \Omega, \sigma^2, C^P, C^{PET}) = (2 \times \pi \times \sigma^2)^{-\frac{T}{2}} \prod_{t=1}^{T} \exp\left(-\frac{(Q_t - \widehat{Q}_t)^2}{2 \times \sigma^2}\right) \tag{9}$$

where ω_{ζ_2} and c_{ζ_2} are equal to $\frac{\Gamma^{1/2}[3(1+\zeta_2)/2]}{(1+\zeta_2)\Gamma^{\frac{3}{2}}[(1+\zeta_2)/2]}$ and $\left(\frac{\Gamma[3(1+\zeta_2)/2]}{\Gamma[(1+\zeta_2)/2]}\right)^{1/(1+\zeta_2)}$, respectively. The values of $\alpha_{\zeta_1,t}$ and ξ_ζ are computed as a function of two parameters (ζ_1 and ζ_2) as detailed in Schoups and Vrugt (2010).

3.3. Frequency analysis modeling

Fitting of a pdf is required to estimate the frequency of projected flow and leads to a systematic procedure for extrapolation to frequencies beyond the range of the data set. Appropriate selection of the distribution is important – this study determines a reasonable distribution using three goodness of fit tests (Kolmogorov-Smirnov, Anderson-Darling, and upper tail Anderson-Darling). When the distribution is selected, the parameter set ψ of that distribution is estimated so that required quantiles can be estimated with the fitted model. To consider uncertainty of the parameter set in the frequency analysis, the estimation of the parameter set is performed in a Bayesian framework using vague uniform distributions as priors.

3.4. Framework to quantify climate change impact on hydrologic response

A flowchart of the proposed statistical framework is presented in Fig. 2. Note that this study does not investigate all related uncertainties

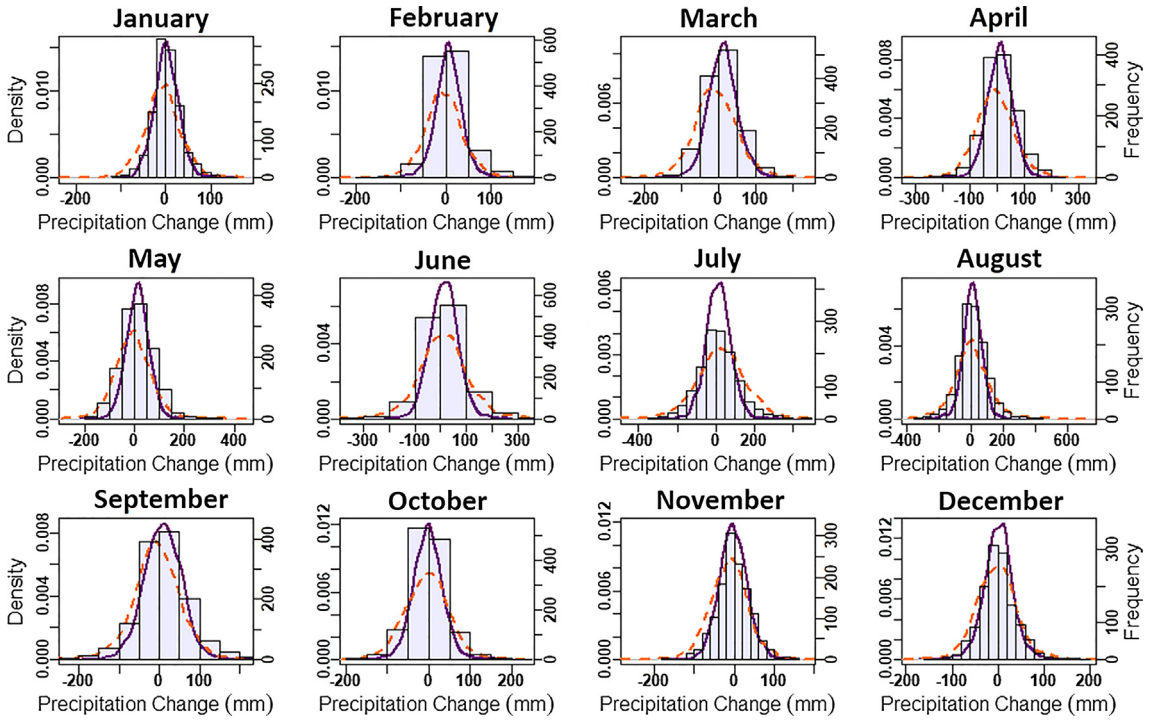

Fig. 3. Posterior densities for future monthly precipitation change (2060 target year) for the study area developed with (red dashed) and without (blue solid) accounting of intermodel correlations. The histograms of monthly precipitation change computed directly from the climate model output are also presented. (For interpretation of the references to color in this figure legend, the reader is referred to the web version of this article.)

in future hydrologic projections. For instance, we do not address the uncertainty of emission scenarios which has been considered one of the main uncertainty sources (Fang et al., 2015; Ficklin et al., 2016). Rather, the framework aims to demonstrate how future hydrologic response is affected to describe robust future integrated uncertainty by the different definitions of the climate ensemble and hydrologic error model. We aim to quantify the effect of three main sources, namely climate projections (CP), hydrologic modeling (HM), and frequency analysis (FA) uncertainties in inferred quantiles of future streamflow.

In total, four models ($M_{S_\times E}$, $M_{S_O E}$, $M_{S_\times E_t}$, and $M_{S_O E_t}$) are developed. The subscripts $S_\times$ and S_O denote estimates without and with inclusion of intermodal similarities, respectively. The subscripts E and E_t indicate a normal likelihood function and probabilistic error models, respectively. Therefore, the first model, $M_{S_\times E}$, estimates future streamflow based on a climate model without accounting for intermodel similarities as well as the hydrologic model with a normal likelihood function. In the second model, $M_{S_O E}$, future streamflow is estimated by a climate model while accounting for intermodel similarities and the hydrologic model with a normal likelihood function. The third model ($M_{S_\times E_t}$) adopts a hydrologic model with a probabilistic error model but does not consider intermodel similarities in a climate model. Lastly, the fourth model ($M_{S_O E_t}$) includes both a climate model with accounting for intermodel similarities and a hydrologic model along with a probabilistic error model.

The framework for all models is as follows.

[1] After future climate changes (M_{S_O} and $M_{S_\times}$) are identified using Eq. (1) with the definitions in the covariance matrix, G climate scenarios (G = 800 in this study) are generated for a climate sequence time length T (T = 30years × 365days for this study) using the weather generator as stated in Section 3.1.

[2] The hydrologic models ($M_{E_t}$and M_E) are calibrated/evaluated using historical data and then K parameter sets (K = 800 for each model) are obtained from the posterior distributions. Here, the hydrologic error models are constructed by the definitions (Eq. (3)).

[3] Projected streamflows (Q_t) are independently developed using the g^{th} scenario of future climate and k^{th} hydrologic parameter set $\Omega_k^{GR4J} = \{\Omega_{1,k}, \Omega_{2,k}, \Omega_{3,k}, \Omega_{4,k}\}$ for $M_{E_t}$and M_E independently.

[4] To develop the final streamflow projections, samples of T perturbations $\varepsilon = \{\varepsilon_1, \varepsilon_2, \cdots, \varepsilon_T\}$ from each model (M_{E_t}or M_E) are generated using k^{th} error model parameter set $\Omega_k^{\varepsilon} = \{\vartheta_{0,k}, \vartheta_{1,k}, \zeta_{1,k}, \zeta_{2,k}\}$ or $\{\sigma_k^2\}$.

[5] Streamflow statistics Y_p (i.e., the p^{th} percentile) are calculated through the optimal probability distribution. To account for sampling error, draw W estimates (W = 600 in this study) of probability model parameters $\psi_{\boldsymbol{w}}$. This study estimates the frequency of monthly maxima flow using the Generalized Extreme Value (GEV) distribution (i.e., $\psi_{\boldsymbol{w}} = \{\psi_{location,w}, \psi_{scale,w}, \psi_{shape,w}\}$). The GEV was selected after various alternatives (Generalized Extreme Value, Generalized Pareto (GP), normal, lognormal, exponential, and Weibull distributions) were considered.

[6] Rather than running steps [3]–[5] for all G × K × W simulations, we minimize computation time by selecting a random sample of N simulations (N = 3000 in this study) with climate projection g ∈ G, hydrologic model parameter sets k ∈ K, and frequency analysis sets w ∈ W. We also note that the values of K, W, and N are sufficiently large compared to those of previous studies (Qi et al., 2016; Wilby and Harris, 2006).

[7] The expected value of streamflow statistics $Y_{w,p}$ can be calculated by taking the mean, $\bar{Y}_p$. Similarly, predictive intervals $\left[Y_{p\frac{\alpha}{2}}, Y_{p\left(1-\frac{\alpha}{2}\right)}\right]$ can be developed using the $\frac{\alpha}{2}$ and $\left(1-\frac{\alpha}{2}\right)$ percentiles of the ensemble estimates. Note that uncertainty of the various sources is not independent from each other and thus not necessarily additive (Montanari and Koutsoyiannis, 2012; Sikorska and Renard, 2017), indicating that integrated uncertainty is usually not equal to the sum of its contributing sources. Therefore, this study directly compares individual uncertainties that are involved and propagated in integrated uncertainty after considering all sources of uncertainty.

4. Results

4.1. Monthly climate simulations from expected changes

Probability density functions (pdfs) are fitted to the monthly climate data generated by the RCP 8.5 scenarios with and without accounting for the intermodel correlations. Fig. 3 shows pdfs of monthly precipitation change for the study area. Figs. S1 and S2 in the supporting information present monthly change for maximum and minimum temperatures, respectively. The histograms of monthly change computed directly from the climate model output are also presented to highlight that our probability models used to represent climate change provide similar results with the empirical changes. Including intermodel correlations reduces the effective number of data points and accentuates differences between models such that an increase in variance is prevalent across all months and variables. For example, the variance of a precipitation increase in March significantly is increased from 1430 to 3220 after intermodel correlations are included. Similarly, the variance without accounting for model similarities is 1960 in May whereas precipitation is more uncertain (variance = 5320) after intermodel correlations are considered. Temperature uncertainties are also increased since temperature data are substantially correlated. Beyond the increased variance of projected changes, the mean estimates are also shifted due to intermodel correlations. For instance, the mean of precipitation change in February increases by 7.8 mm without considering model similarities, while precipitation decreases by 7.2 mm on average when intermodel correlations are considered. This is because the entire data are no longer regarded as an independent data set, allowing that a model showing less correlation is provided more weight in the calculation. In particular, this is seen in the precipitation for winter months (i.e., January and February).

The pdfs of climate change can be used to evaluate changes in hydrologic response in the study area, in which a stochastic weather generator is used to generate an ensemble of daily climate time series. Before generating a climate time series, the capability of the stochastic weather generator is evaluated by reproducing historic climate conditions. In this evaluation, 800 simulations with no changes imposed are compared against observed statistics (Fig. 4). The average, standard deviation, skew of daily precipitation, and the average lengths of wet spells for each month are presented in Fig. 4a–d. Similarly, the average and standard deviation of maximum/minimum temperatures are shown in Fig. 4e–f. In general, the results suggest good performance using all variables and statistics but the simulations slightly underestimate the average lengths of wet spells for some months (e.g., July, August, and September). Also, the model exhibits bias with regards to standard deviations of maximum/minimum temperatures for some months (e.g., January and September). We also confirm that the cross-correlations of all variables for each month are fairly preserved in the simulations (not shown). Overall, the performance suggests that the model is appropriate to reproduce climate scenarios for the study area. Finally, using the weather generator, 800 different 30-year climate daily simulations are developed with different changes imposed.

4.2. Hydrologic model calibration and evaluation

The simulated streamflow in the Yongdam Basin was not significantly autocorrelated (see Fig. S3a) so ϑ_2 was excluded and our model was calibrated by δ_t $SEP(0, 1, \zeta_1, \zeta_2)$. Fig. 5 shows the simulated daily streamflow for a portion of the calibration and validation periods by GR4J incorporating the two predictive error models (M_E and M_{E_t}). Note that negative predictions are set to zero. Table 1 presents summaries of the prior and posterior distributions of M_{E_t} for the Yongdam Basin. Figs. S3b and S3c present diagnostic plots to demonstrate the usefulness of the fitted error model over the validation period.

The Nash-Sutcliffe Efficiency (NSE), R^2, and mean error (ME) for simulated streamflow using the median parameter set of M_{E_t} equal 0.76, 0.78, and −0.47 mm for the calibration period and 0.88, 0.90, and −0.71 mm for the validation period. These performances are considered either “good” or “acceptable” based on performance criteria suggested by Martinez and Gupta (2010). Note that because none of these statistics are adopted for the calibration objective, they are not significantly decreased from the calibration to the validation period. Rather, the statistics are improved in the validation period. Fig. 5a presents 90% credible bounds for simulated streamflow. Credible intervals include observed values 87.6% (91.33%) in the calibration (validation) period, indicating that the error model of M_{E_t} is appropriate to represent residual error uncertainty. Also, when the two residual models (M_E and M_{E_t}) are compared, there are only negligible differences in terms of mean predictive performance (Fig. 5b and c), with slight improvement under M_{E_t}. However, the quantification of predictive uncertainty of M_E may not be realistic. While the credible bounds of high flow may be underestimated in M_E, the intervals of low flow seem to be overestimated (see Fig. 5b). The credible bounds in M_E provide significant bias in the frequency analysis (presented in Section 4.3). Fig. S3b shows the fitted and empirical density functions in M_{E_t} which support our inference. The fitted density function captures the skewness of the errors although it has some bias in the peakedness. Fig. S3c presents the relationship between predicted streamflow and residual errors in both models. While the variance of the residuals in M_E increases significantly with the magnitude of predicted flow, heteroscedasticity is apparently removed in the residuals of M_{E_t}.

4.3. Inter-model comparison in quantifying future projections

Streamflow changes in each month are investigated with and without accounting for intermodel correlations (Fig. 6). Each box has 720,000 daily streamflow simulations based on each climate change definition ($M_{S_\times}$ and M_{S_O}). Here, hydrologic uncertainty is not considered to emphasize differences in accordance with climate change definitions. The results clearly show changes particularly for mean estimates in JAS when intermodel correlations are included. For example, the mean of daily streamflow in August is 4.01 mm without considering model similarities, while streamflow is 3.54 mm on average, when intermodel correlations are considered. Also, mean streamflow in July is decreased by 0.5 mm after intermodel correlations are included. Streamflow changes in summer months are further analyzed in Section 4.3. Overall, analysis indicates that streamflow projections can vary with and without accounting for intermodel correlations.

Next, integrated 95% predictive intervals for quantiles of maximum daily streamflow are investigated. Future daily maximum statistics (Y) for February and August are selected since they experience a widespread range of alterations under climate change, the statistics for these months are selected. Fig. 7 shows the integrated uncertainties of climate projections, hydrologic modeling, and frequency analysis uncertainty for the quantiles of August streamflow. Based on four models ($M_{S_\times E}$, $M_{S_O E}$, $M_{S_\times E_t}$, and $M_{S_O E_t}$), the values in the p^{th} percentile of daily maximum streamflow are estimated following the GEV distribution. CP uncertainties are developed by the ensemble of climate scenarios run over the median parameter sets of hydrologic and frequency models without adding residual noise. Integration of CP and HM is made by simultaneously considering ensemble climate scenarios and residual uncertainty in the hydrologic model. Integrated uncertainty (CP, HM and FA) is developed by incorporating frequency analysis uncertainty as well. Table 2 presents the median quantiles estimated for the main percentiles of August maximum streamflow. Then, Fig. 8 presents the relative contributions among three contributing sources. Each contribution is estimated by the ratio of differences calculated with the standard deviations of the three sources.

Several insights emerge from Figs. 7, 8 and Table 2. First, CP uncertainty is the largest in low- and medium percentiles, indicating that the projected value of future streamflow is mainly determined for those percentiles by climate information. However, its relative contribution is

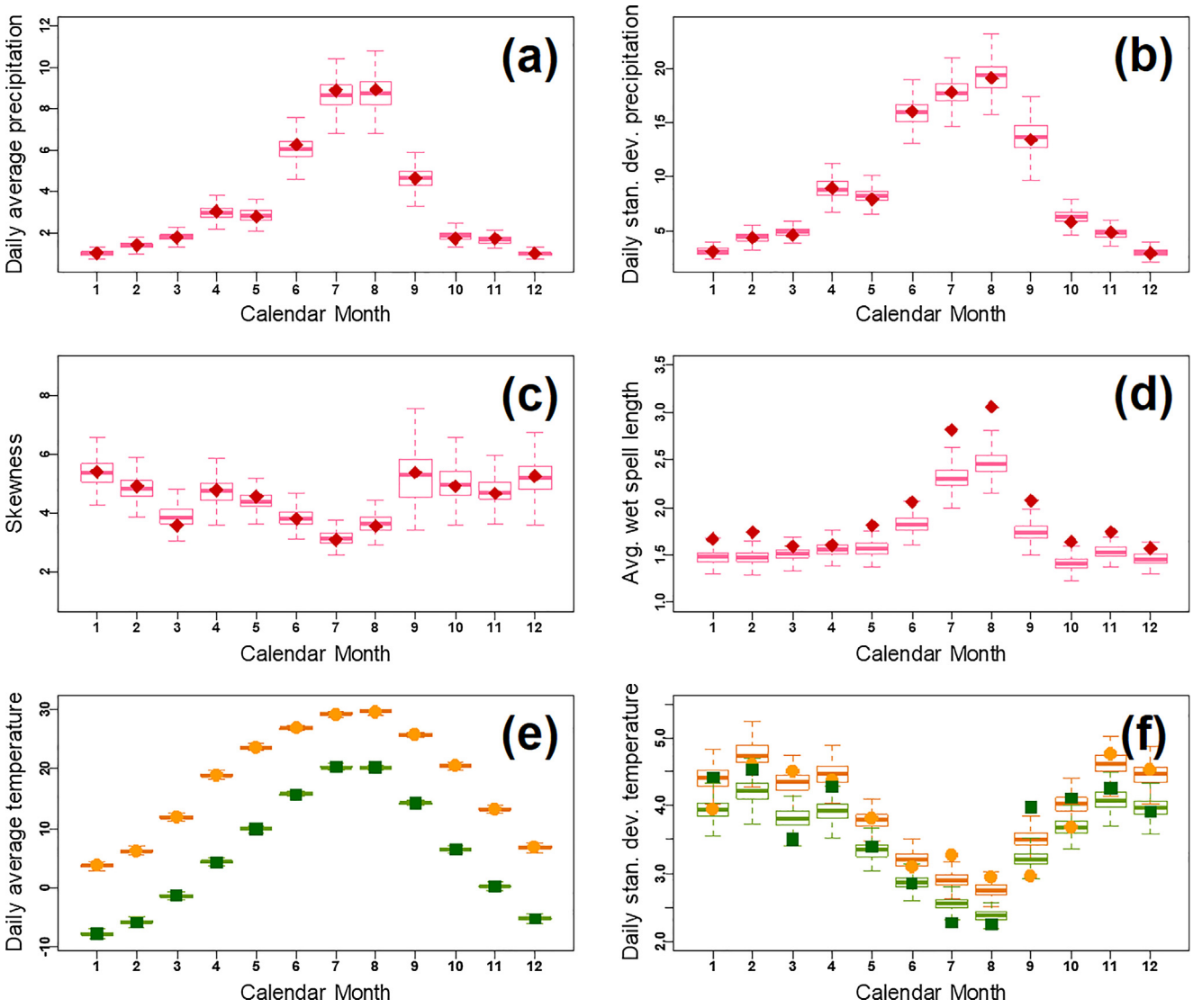

Fig. 4. Evaluation of historical climate simulations, including the (a) average (b) standard deviation (c) skewness (d) wet spell length for basin precipitation (e) average and (f) standard deviation for maximum (yellow) and minimum (green) temperatures. Box plots represent the model performances across 800 simulations of 30 years each. Observed statistics (precipitation, maximum and minimum temperatures) are also presented by diamond, circle, and rectangle, respectively. (For interpretation of the references to color in this figure legend, the reader is referred to the web version of this article.)

decreased in high percentiles whereas the importance of HM and FA uncertainty is increased. This is a particularly important point. The hydrologic modeling and frequency processes are nonlinear so different parameterizations of those models and their combinations will result in various responses to a given climate. When uncertainty quantification analysis is conducted, the investigators must be careful with the nonlinearity.

The intermodel correlations shift the mean estimates in the projected inferred quantiles of August maximum flows. The mean values in all quantiles are increased up to 8.1% after intermodel correlations are considered (M_{S_XE} vs. M_{S_OE} in Table 2). Also, accounting for intermodel correlation provides changes in predictive bounds. CP uncertainty in M_{S_OE} is significantly increased when compared to M_{S_XE}. For instance, relative CP uncertainties in M_{S_XE} are 0.85 and 0.65 at 30% and 90% probabilities whereas the uncertainties in M_{S_OE} are 0.93 and 0.75, respectively. Both differences are due mainly to an increase in the variances and mean changes in the pdfs of August precipitation as seen in Fig. 3. This finding indicates that CP uncertainty may be too narrow if intermodel similarities are not considered in defining climate scenarios. Third, HM uncertainty in M_{S_XE} is significantly more underestimated than that in $M_{S_XE_t}$. Underestimation is also prevalent in M_{S_OE}, highlighting that the simple error model used in quantifying uncertainty through climate impact assessments of hydrologic response may be limited to representing precise hydrologic uncertainty. Many studies have concluded that hydrologic uncertainty represents just a small portion (less than5%) of integrated uncertainty for all percentiles (Lee et al., 2017; Teng et al., 2012) which is the same conclusion when M_E is used. However, relative HM uncertainty is significantly increased (up to 18%) when M_{E_t} is applied.

As we noted in Section 4.2, the credible bounds of high flow in M_E are underestimated while the credible bounds of high flow in M_{E_t} may be realistic. Accordingly, when the medians in percentiles are estimated in Table 2, values of the M_E are substantially less than M_{E_t}. We also confirm another limitation when M_E is utilized in the lower percentiles. Fig. 9 shows the integrated uncertainties of climate projections, hydrologic, and frequency analysis for quantiles of February streamflow. Here, the lower bounds of the integrated predictive intervals for integrated uncertainty ("CP, HM and FA") in Fig. 9b and 9d are almost equivalent to those for the others ("CP" and "CP and HM"). In Fig. 9a and c, the CP uncertainties show a completely different pattern when

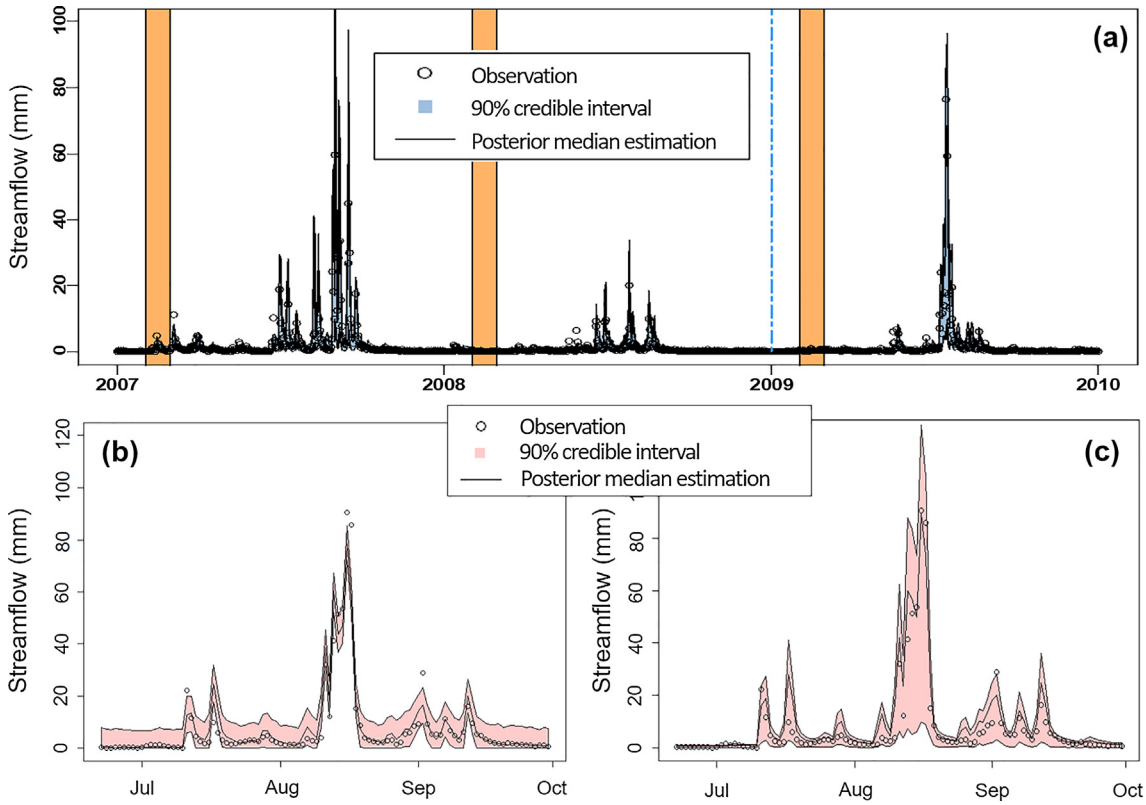

Fig. 5. The posterior median estimates and 90% credible intervals for the calibration and validation periods (The February period is highlighted with yellow). (a) Simulated flow under M_{E_t} from Jan. 2007 to Dec. 2009, (b) and (c) Simulated flow in 2010 under M_E and M_{E_t}, respectively. (For interpretation of the references to color in this figure legend, the reader is referred to the web version of this article.)

compared to other uncertainty sources, which is not realistic. The CP uncertainties are developed by running the ensemble of climate scenarios through the median parameter sets of hydrologic and frequency models without adding any residual noise. While February is generally a low flow period (see yellow boxes presented in Fig. 5), maximum flow in that month is determined mainly by the hydrologic modeling process. In particular, the residual model plays a crucial role in determining extremes by adding errors. Adopting a simple error model provides biased predictive intervals for low flow with extreme overestimations, highlighting the importance in the choice of a residual model.

4.4. Comparison between $M_{S_O E_t}$ projections and baseline response

After investigating changes in the cumulative uncertainties by the comparing four models ($M_{S_x E}$, $M_{S_O E}$, $M_{S_x E_t}$, and $M_{S_O E_t}$) developed in this study, we determine the predictive bounds in quantiles of future streamflow by considering climate model similarity and hydrologic error uncertainty. Then, the cumulative uncertainties of quantile estimates are directly compared on historic and future streamflow based on $M_{S_O E_t}$. Fig. 10 presents the cumulative uncertainty in the Yongdam Basin for three months (February, July and October) to highlight differences between historic and future bounds. The cumulative 95% predictive intervals of integrated uncertainty are employed to compare two periods. Here, historical cumulative uncertainty is built using observed climate conditions (1975–2004) so it includes hydrologic and frequency analysis uncertainties. If two predictive intervals of flow quantiles are less overlaid, it indicates that flow quantiles will differ under future climate conditions.

Fig. 10a presents the cumulative estimates for February maximum streamflow. The range of future projections differs little from historical streamflow although the spread in future periods for most quantiles extends both below and above those of historical periods. These results suggest that no significant change in most February flow quantiles is

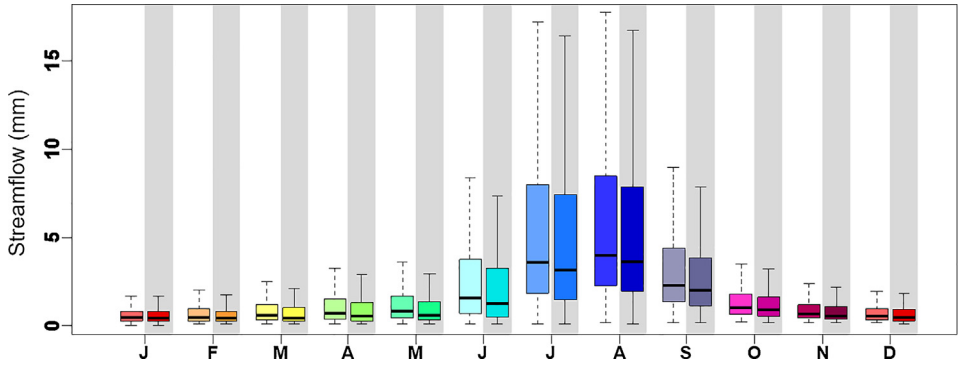

Fig. 6. Box plots for future streamflow generated by two climate change definitions (M_{S_X} and M_{S_O}). Monthly streamflow of M_{S_O} is highlighted (gray color).

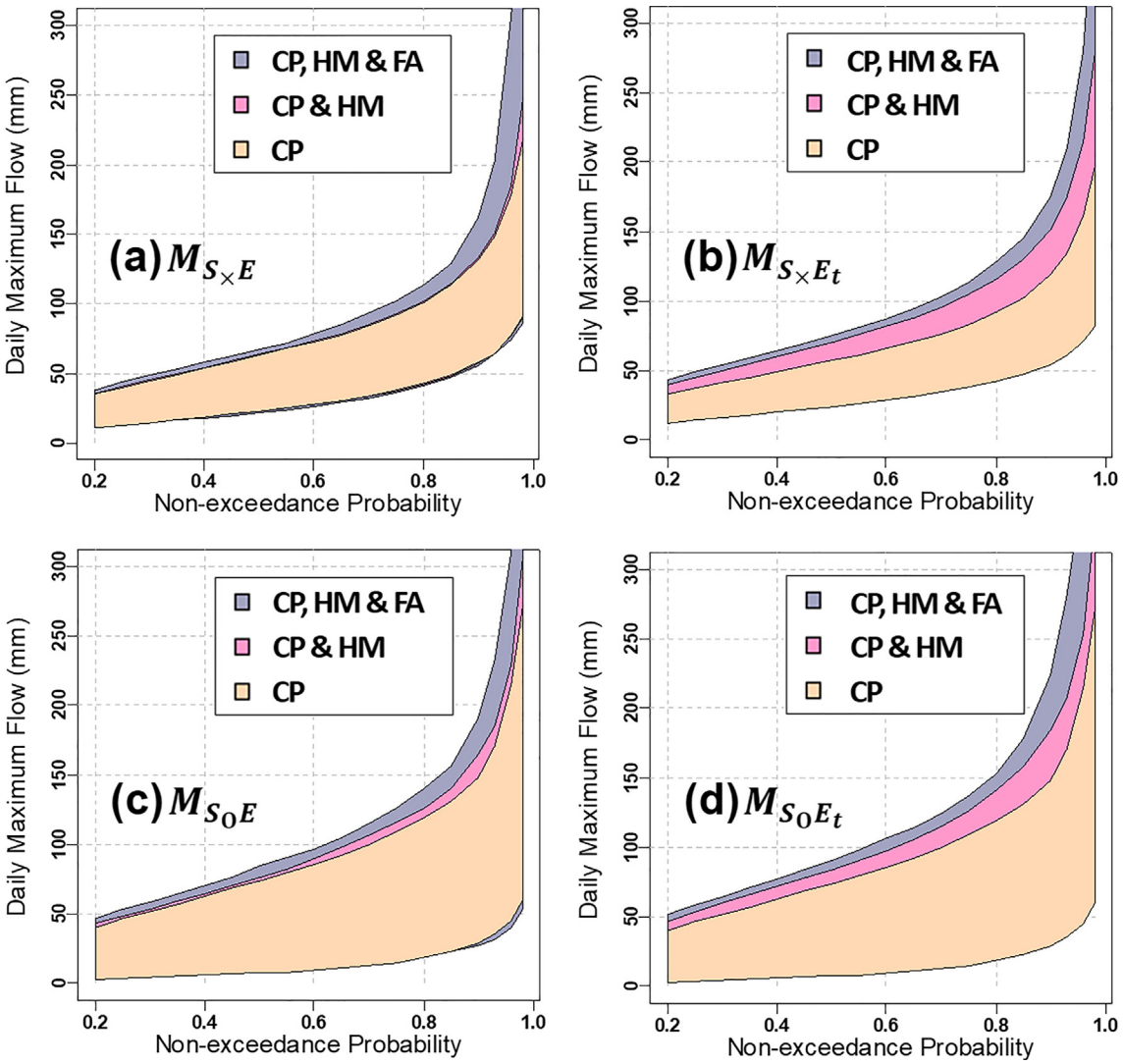

Fig. 7. Integrated 95% predictive intervals for quantiles of August maximum streamflow in the future. Climate projection (CP), the integration of climate projection and hydrologic modeling uncertainties (CP & HM) are presented. Also, the cumulative uncertainty after frequency analysis uncertainty (CP, HM & FA) is included.

projected in the set of CMIP5. Fig. 10b presents results for July maximum streamflow. The projections may show July flows increasing in a lower quantile while flows in a higher quantile may be decreased although they are still in predictive bounds. Results indicate that lower flows are expected in the future than in the present, likely due to changes reflecting the extraordinarily high rainfall in summer. Over most July quantiles, approximately 47% of the bounds for future uncertainties lie outside the range of historical uncertainty. Fig. 10c shows that there are meaningful differences between the distribution of October maximum streamflow in the historical and future periods. Fig. 10c presents results for October maximum streamflow. The projections show October flows increasing in a higher quantile while flows in a lower quantile may be unchanged. This suggests that this region requires more careful planning of water management for this month in the future.

5. Summary and conclusions

Using a proposed framework, this study explores the magnitude and sources of uncertainty in future hydrologic projections. The framework allows propagating uncertainty among future climate, hydrologic modeling and frequency analysis and determining integrated uncertainty bounds based on defined uncertainty sources. A series of nested formulations ($M_{S_{\times}E}$, M_{S_OE}, $M_{S_{\times}E_t}$, and $M_{S_OE_t}$) is developed to examine uncertainties arising from (1) climate models with and without accounting of intermodel similarities and (2) a hydrological model with

Table 2
The median estimates of the total integrated uncertainty estimated for the 25th, 50th, 70th, 90th, and 98th percentiles in August maximum streamflow by four models. Relative changes from $M_{S_{\times}E}$, $(Y_p^M - Y_p^{M_{S_{\times}E}})/Y_p^{M_{S_{\times}E}}$, are also presented in the parenthesis.

Percentile Model	25th	50th	70th	90th	98th
$M_{S_{\times}E}$	26.32 (0.00)	42.65 (0.00)	59.27 (0.00)	93.44 (0.00)	146.31 (0.00)
$M_{S_{\times}E_t}$	29.57 (0.123)	48.30 (0.132)	67.67 (0.141)	107.09 (0.146)	169.56 (0.159)
M_{S_OE}	23.84 (−0.094)	40.49 (−0.050)	58.16 (−0.018)	95.54 (0.023)	158.23 (0.081)
$M_{S_OE_t}$	27.97 (0.062)	46.89 (0.099)	66.67 (0.124)	109.11 (0.167)	178.11 (0.217)

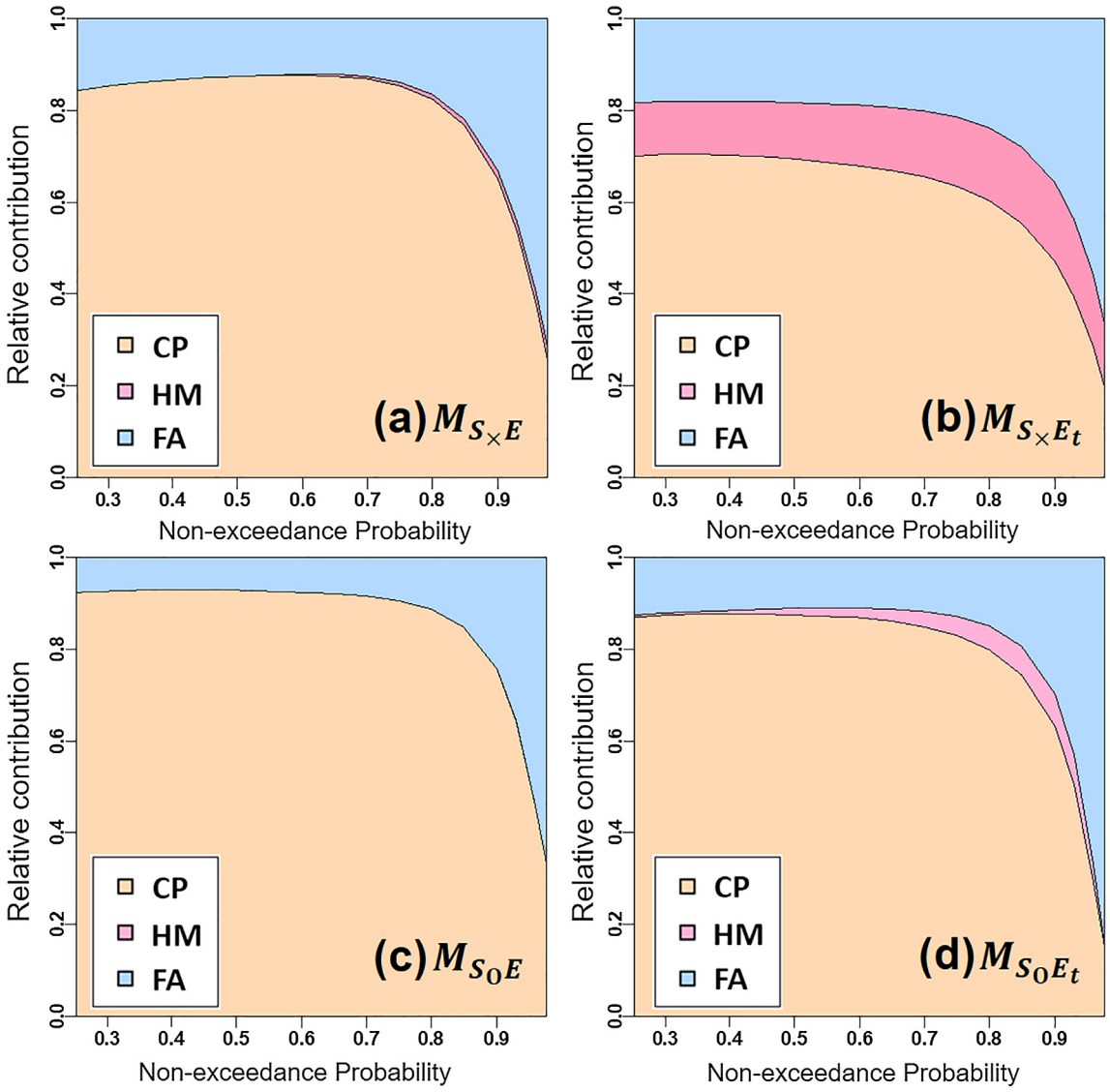

Fig. 8. Relative contributions among climate projection (CP), hydrologic modeling (HM), and frequency analysis (FA) uncertainties for July maximum streamflow. Each contribution is defined as the ratio of differences calculated with the standard deviations for the integrated 95% predictive intervals (presented in Fig. 6).

two different error model definitions, which have previously received less attention in studies propagating uncertainty through climate change impacts on hydrologic alteration.

Results from a case study of the Yongdam Basin demonstrate how comprehensive uncertainty can be affected by defining each uncertainty source. Variance in hydrologic response can be underestimated if similarities in climate models are not considered. Furthermore, accounting for intermodel correlations offers different results in climate change analysis for the region. These findings may suggest there is biased information in the approaches of multi-model climate ensembles, which have been commonly used in previous studies. When compared to the simple error model for the hydrologic predictive errors, the residual model adopting autocorrelation, heteroscedasticity, and non-normality incorporates significantly more of the integrated uncertainty of future streamflow frequency. Although climate information and frequency analysis represent the most influential sources of uncertainty, our results indicate that hydrologic uncertainty should not be ignored in studies investigating uncertainty analysis of hydrologic alteration under climate change. Lastly, we find that the simple definition of the hydrologic error model can provide critical bias in determining the inferred quantiles of future streamflow. Our definitions of the uncertainty sources could be very valuable in facilitating decisions of water resource planners by providing possible hydrologic changes to future climate.

While these results are important, there are a number of issues requiring further discussion. Our study does not purport to investigate completely integrated uncertainties in climate change assessment, indicating that the uncertainty of each component adopted here could be altered when full analysis is considered. For instance, Sharma et al. (2018) and Teutschbein et al. (2011) demonstrate that downscaling approaches are comparable to or more important than the GCMs themselves. Also, only one hydrological model structure is used in this study even though model structure is also an important source of hydrologic uncertainty (Mockler et al., 2016; Poulin et al., 2011). Lastly, Chen and Brissette (2017) report that uncertainty is substantially increased when a simple interpolation method is adopted in manipulating climate outputs, as was also used in this study.

Perhaps a larger limitation of this study is linked to the formulation and concept of a probability model for defining climate change. The probability model determines changes in climate variables by considering intermodel correlations, which means that the model provides extra weight to a model which has a very different response to other models. This could be a limitation if there is a poorly performing model. It may be desirable to apply a model selection method prior to

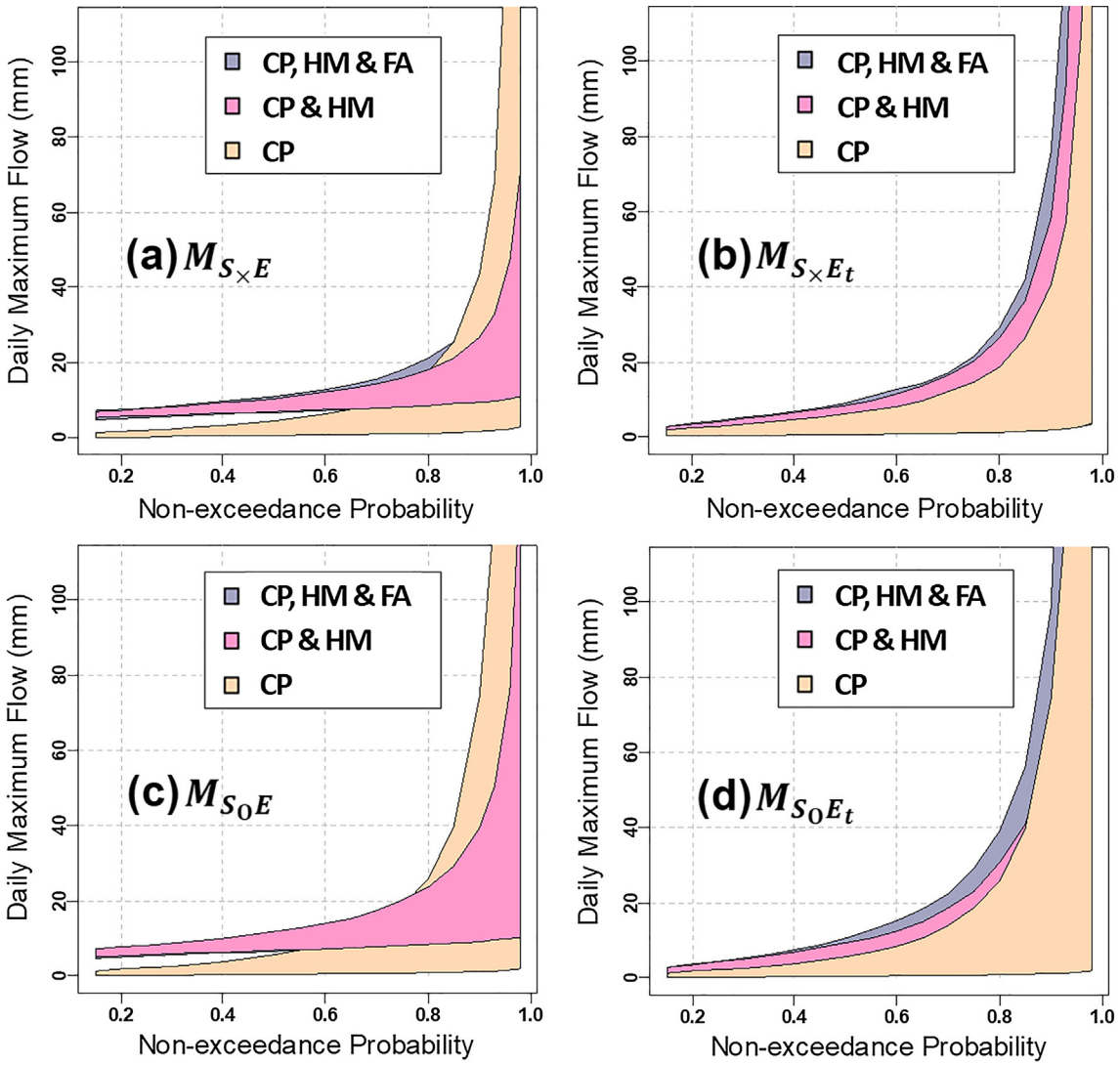

Fig. 9. Integrated 95% predictive intervals for quantiles of February maximum streamflow in the future. Climate projection (CP), the integration of climate projection and hydrologic modeling uncertainties (CP & HM) and the integration of climate projection, hydrologic modeling, and frequency analysis uncertainties (CP, HM & FA) are presented.

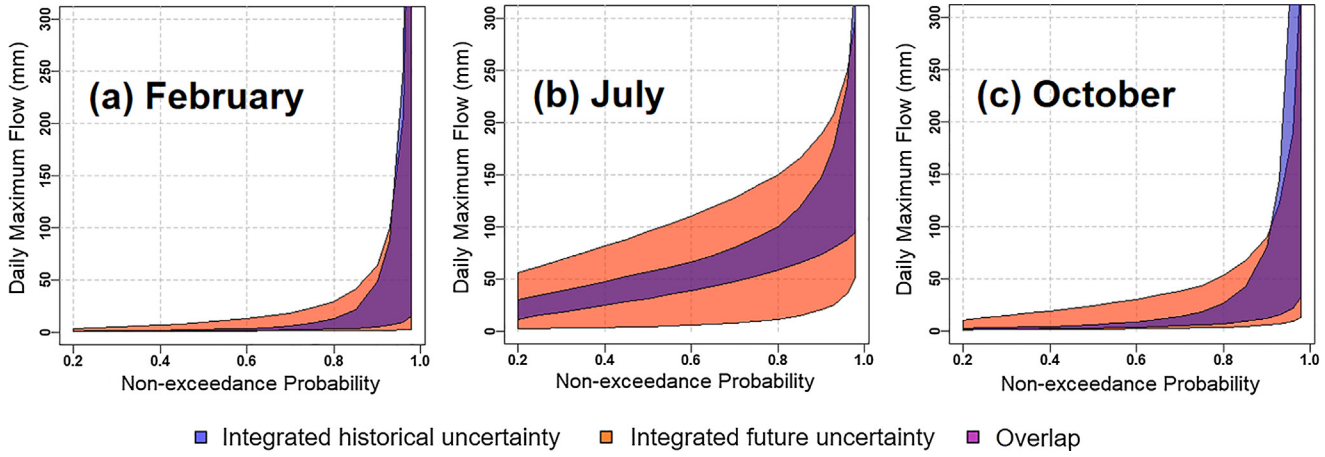

Fig. 10. Integrated 95% predictive intervals in maximum flow quantiles for historical and future periods for the months of (a) June, (b) July, and (c) October.

propagating climate model uncertainty. The framework presented here underscores the importance of the definitions of each component adopted here for climate change assessment.

Future work will examine in detail some of the components used in this study. Model similarity of individual climatic variables (e.g., precipitation or temperature) can provide a different level of uncertainty. Also, individual components in hydrologic uncertainty (e.g., model structure, parameters, and error model) contribute differentially to integrated uncertainty. Future work will also require applying the methodology presented here to other watersheds. Uncertainty of climate change impacts may vary among regions due to various hydroclimatologic conditions and combinations between climate simulations and regional conditions (Ahn et al., 2016). It would be worthwhile to work towards drawing more generalized conclusions.

Acknowledgments

The authors are grateful to three anonymous reviewers and the Associate Editor for their thoughtful insights and useful suggestions.

Appendix A. Supplementary data

Supplementary data to this article can be found online at https://doi.org/10.1016/j.jhydrol.2018.12.061.

References

Abramowitz, G., Bishop, C., 2015. Climate model dependence and the ensemble dependence transformation of CMIP projections. J. Clim. 28, 2332–2348.
Ahn, K.-H., Merwade, V., Ojha, C.S.P., Palmer, R., 2016. Quantifying Relative Uncertainties in the Detection and Attribution of Human-induced Climate Change on Winter. Streamflow. J. Hydrol.
Akaike, H., 1981. Likelihood of a model and information criteria. J. Econom. 16, 3–14.
Allen, R.G., Pereira, L.S., Raes, D., Smith, M., et al., 1998. Crop evapotranspiration-Guidelines for computing crop water requirements-FAO Irrigation and drainage paper 56. FAO Rome 300, 6541.
Arnell, N.W., Gosling, S.N., 2016. The impacts of climate change on river flood risk at the global scale. Clim. Change 134, 387–401.
Bae, D.-H., Jung, I.-W., Lettenmaier, D.P., 2011. Hydrologic uncertainties in climate change from IPCC AR4 GCM simulations of the Chungju Basin. Korea. J. Hydrol. 401, 90–105.
Beven, K.J., Smith, P.J., Freer, J.E., 2008. So just why would a modeller choose to be incoherent? J. Hydrol. 354, 15–32.
Bosshard, T., Carambia, M., Goergen, K., Kotlarski, S., Krahe, P., Zappa, M., Schär, C., 2013. Quantifying uncertainty sources in an ensemble of hydrological climate-impact projections. Water Resour. Res. 49, 1523–1536.
Brigode, P., Oudin, L., Perrin, C., 2013. Hydrological model parameter instability: a source of additional uncertainty in estimating the hydrological impacts of climate change? J. Hydrol. 476, 410–425.
Chen, J., Brissette, F.P., 2017. Hydrological modelling using proxies for gauged precipitation and temperature. Hydrol. Process. 31, 3881–3897.
Chen, J., Brissette, F.P., Poulin, A., Leconte, R., 2011. Overall uncertainty study of the hydrological impacts of climate change for a Canadian watershed. Water Resour. Res. 47.
Christierson, B., Vidal, V., Wade, S.D., 2012. Using UKCP09 probabilistic climate information for UK water resource planning. J. Hydrol. 424, 48–67.
Cordano, E., Eccel, E., 2016. Tools for stochastic weather series generation in R environment. Ital. J. Agrometeorol.-Riv. Ital. Agrometeorol. 21, 31–42.
Dobler, C., Hagemann, S., Wilby, R., Stötter, J., 2012. Quantifying different sources of uncertainty in hydrological projections in an Alpine watershed. Hydrol. Earth Syst. Sci. 16, 4343–4360.
Edijatno, Yang, N., Makhlouf, X., Michel, Z., 1999. GR3J: a daily watershed model with three free parameters. Hydrol. Sci. J. 44, 263–277.
Etemadi, H., Samadi, S., Sharifikia, M., 2014. Uncertainty analysis of statistical downscaling models using general circulation model over an international wetland. Clim. Dyn. 42, 2899–2920.
Evin, G., Kavetski, D., Thyer, M., Kuczera, G., 2013. Pitfalls and improvements in the joint inference of heteroscedasticity and autocorrelation in hydrological model calibration. Water Resour. Res. 49, 4518–4524.
Evin, G., Thyer, M., Kavetski, D., McInerney, D., Kuczera, G., 2014. Comparison of joint versus postprocessor approaches for hydrological uncertainty estimation accounting for error autocorrelation and heteroscedasticity. Water Resour. Res. 50, 2350–2375.
Fang, G., Yang, J., Chen, Y., Zhang, S., Deng, H., Liu, H., De Maeyer, P., 2015. Climate change impact on the hydrology of a typical watershed in the Tianshan Mountains. Adv. Meteorol.
Ficklin, D.L., Letsinger, S.L., Stewart, I.T., Maurer, E.P., 2016. Assessing differences in snowmelt-dependent hydrologic projections using CMIP3 and CMIP5 climate forcing data for the western United States. Hydrol. Res. 47, 483–500.
Franco, G., Cayan, D.R., Moser, S., Hanemann, M., Jones, M.-A., 2011. Second California Assessment: integrated climate change impacts assessment of natural and managed systems. Guest editorial. Clim. Change 109, 1–19.
Gelman, A., Carlin, J.B., Stern, H.S., Rubin, D.B., 2014. Bayesian data analysis. Taylor & Francis.
Hall, J., Watts, G., Keil, M., De Vial, L., Street, R., Conlan, K., O'Connell, P., Beven, K., Kilsby, C., 2012. Towards risk-based water resources planning in England and Wales under a changing climate. Water Environ. J. 26, 118–129.
Hargreaves, G.H., Samani, Z.A., 1982. Estimating potential evapotranspiration. J. Irrig. Drain. Div. 108, 225–230.
Haughton, N., Abramowitz, G., Pitman, A., Phipps, S.J., 2015. Weighting climate model ensembles for mean and variance estimates. Clim. Dyn. 45, 3169–3181.
Honti, M., Stamm, C., Reichert, P., 2013. Integrated uncertainty assessment of discharge predictions with a statistical error model. Water Resour. Res. 49, 4866–4884.
Jeong, Y.H., Yang, J.S., Park, K., 2014. Changes in water quality after the construction of an estuary dam in the Geum River Estuary Dam system. Korea. J. Coast. Res. 30, 1278–1286.
Karlsson, I.B., Sonnenborg, T.O., Refsgaard, J.C., Trolle, D., Børgesen, C.D., Olesen, J.E., Jeppesen, E., Jensen, K.H., 2016. Combined effects of climate models, hydrological model structures and land use scenarios on hydrological impacts of climate change. J. Hydrol. 535, 301–317.
Kay, A., Davies, H., Bell, V., Jones, R., 2009. Comparison of uncertainty sources for climate change impacts: flood frequency in England. Clim. Change 92, 41–63.
Knutti, R., Masson, D., Gettelman, A., 2013. Climate model genealogy: generation CMIP5 and how we got there. Geophys. Res. Lett. 40, 1194–1199.
Lee, J.-K., Kim, Y.-O., Kim, Y., 2017. A new uncertainty analysis in the climate change impact assessment. Int. J. Climatol. 37, 3837–3846.
Li, L., Diallo, I., Xu, C.-Y., Stordal, F., 2015. Hydrological projections under climate change in the near future by RegCM4 in Southern Africa using a large-scale hydrological model. J. Hydrol. 528, 1–16.
Martinez, G.F., Gupta, H.V., 2010. Toward improved identification of hydrological models: a diagnostic evaluation of the "abcd" monthly water balance model for the conterminous United States. Water Resour. Res. 46.
Masson, D., Knutti, R., 2011. Climate model genealogy. Geophys. Res. Lett. 38.
McInerney, D., Thyer, M., Kavetski, D., Lerat, J., Kuczera, G., 2017. Improving probabilistic prediction of daily streamflow by identifying Pareto optimal approaches for modeling heteroscedastic residual errors. Water Resour. Res. 53, 2199–2239.
Meinshausen, M., Smith, S.J., Calvin, K., Daniel, J.S., Kainuma, M., Lamarque, J.-F., Matsumoto, K., Montzka, S., Raper, S., Riahi, K., et al., 2011. The RCP greenhouse gas concentrations and their extensions from 1765 to 2300. Clim. Change 109, 213.
Mockler, E.M., Chun, K., Sapriza-Azuri, G., Bruen, M., Wheater, H., 2016. Assessing the relative importance of parameter and forcing uncertainty and their interactions in conceptual hydrological model simulations. Adv. Water Resour. 97, 299–313.
Montanari, A., Koutsoyiannis, D., 2012. A blueprint for process-based modeling of uncertain hydrological systems. Water Resour. Res. 48.
Nguyen, H., Mehrotra, R., Sharma, A., 2016. Correcting for systematic biases in GCM simulations in the frequency domain. J. Hydrol. 538, 117–126.
Pennell, C., Reichler, T., 2011. On the effective number of climate models. J. Clim. 24, 2358–2367.
Perrin, C., Michel, C., Andréassian, V., 2003. Improvement of a parsimonious model for streamflow simulation. J. Hydrol. 279, 275–289.
Plummer, M., et al., 2003. JAGS: A program for analysis of Bayesian graphical models using Gibbs sampling. In: Proceedings of the 3rd International Workshop on Distributed Statistical Computing. Technische Universit at Wien, pp. 125.
Poulin, A., Brissette, F., Leconte, R., Arsenault, R., Malo, J.-S., 2011. Uncertainty of hydrological modelling in climate change impact studies in a Canadian, snow-dominated river basin. J. Hydrol. 409, 626–636.
Qi, W., Zhang, C., Fu, G., Zhou, H., Liu, J., 2016. Quantifying uncertainties in extreme flood predictions under climate change for a medium-sized basin in Northeastern China. J. Hydrometeorol. 17, 3099–3112.
Quintero, F., Mantilla, R., Anderson, C., Claman, D., Krajewski, W., 2018. Assessment of changes in flood frequency due to the effects of climate change: implications for engineering design. Hydrology 5, 19.
Renard, B., Kavetski, D., Leblois, E., Thyer, M., Kuczera, G., Franks, S.W., 2011. Toward a reliable decomposition of predictive uncertainty in hydrological modeling: characterizing rainfall errors using conditional simulation. Water Resour. Res. 47.
Ryu, J.H., Lee, J.H., Jeong, S., Park, S.K., Han, K., 2011. The impacts of climate change on local hydrology and low flow frequency in the Geum River Basin. Korea. Hydrol. Process. 25, 3437–3447.
Sanderson, B.M., Knutti, R., Caldwell, P., 2015. Addressing interdependency in a multimodel ensemble by interpolation of model properties. J. Clim. 28, 5150–5170.
Schoups, G., Vrugt, J.A., 2010. A formal likelihood function for parameter and predictive inference of hydrologic models with correlated, heteroscedastic, and non-Gaussian errors. Water Resour. Res. 46.
Seo, S.B., Kim, Y.-O., Kim, Y., Eum, H.-I., 2018. Selecting climate change scenarios for regional hydrologic impact studies based on climate extremes indices. Clim. Dyn. 1–17.
Sharma, T., Vittal, H., Chhabra, S., Salvi, K., Ghosh, S., Karmakar, S., 2018. Understanding the cascade of GCM and downscaling uncertainties in hydro-climatic projections over India. Int. J. Climatol. 38, e178–e190.
Shen, M., Chen, J., Zhuan, M., Chen, H., Xu, C.-Y., Xiong, L., 2018. Estimating uncertainty and its temporal variation related to global climate models in quantifying climate change impacts on hydrology. J. Hydrol. 556, 10–24.
Sikorska, A.E., Renard, B., 2017. Calibrating a hydrological model in stage space to account for rating curve uncertainties: general framework and key challenges. Adv.

Water Resour. 105, 51–66.
Sivakumar, B., Singh, V., 2012. Hydrologic system complexity and nonlinear dynamic concepts for a catchment classification framework. Hydrol. Earth Syst. Sci. 16, 4119.
Smith, T., Sharma, A., Marshall, L., Mehrotra, R., Sisson, S., 2010. Development of a formal likelihood function for improved Bayesian inference of ephemeral catchments. Water Resour. Res. 46.
Steinschneider, S., McCrary, R., Mearns, L.O., Brown, C., 2015a. The effects of climate model similarity on probabilistic climate projections and the implications for local, risk-based adaptation planning. Geophys. Res. Lett. 42, 5014–5044.
Steinschneider, S., Polebitski, A., Brown, C., Letcher, B.H., 2012. Toward a statistical framework to quantify the uncertainties of hydrologic response under climate change. Water Resour. Res. 48.
Steinschneider, S., Wi, S., Brown, C., 2015b. The integrated effects of climate and hydrologic uncertainty on future flood risk assessments. Hydrol. Process. 29, 2823–2839.
Sun, R., Yuan, H., Liu, X., 2017. Effect of heteroscedasticity treatment in residual error models on model calibration and prediction uncertainty estimation. J. Hydrol. 554, 680–692.
Sun, S., Bertrand-Krajewski, J.-L., 2013. Separately accounting for uncertainties in rainfall and runoff: Calibration of event-based conceptual hydrological models in small urban catchments using Bayesian method. Water Resour. Res. 49, 5381–5394.
Taylor, K.E., Stouffer, R.J., Meehl, G.A., 2012. An overview of CMIP5 and the experiment design. Bull. Am. Meteorol. Soc. 93, 485–498.
Teng, J., Vaze, J., Chiew, F.H., Wang, B., Perraud, J.-M., 2012. Estimating the relative uncertainties sourced from GCMs and hydrological models in modeling climate change impact on runoff. J. Hydrometeorol. 13, 122–139.
Teutschbein, C., Wetterhall, F., Seibert, J., 2011. Evaluation of different downscaling techniques for hydrological climate-change impact studies at the catchment scale. Clim. Dyn. 37, 2087–2105.
Thiessen, A.H., 1911. Precipitation averages for large areas. Mon. Weather Rev. 39, 1082–1089.
Troin, M., Arsenault, R., Martel, J.-L., Brissette, F., 2017. Uncertainty of hydrological model components in climate change studies over two Nordic Quebec catchments. J. Hydrometeorol.
Van Huijgevoort, M., Van Lanen, H., Teuling, A., Uijlenhoet, R., 2014. Identification of changes in hydrological drought characteristics from a multi-GCM driven ensemble constrained by observed discharge. J. Hydrol. 512, 421–434.
Vieux, B.E., Park, J.-H., Kang, B., 2009. Distributed hydrologic prediction: sensitivity to accuracy of initial soil moisture conditions and radar rainfall input. J. Hydrol. Eng. 14, 671–689.
Viglione, A., Merz, R., Salinas, J.L., Blöschl, G., 2013. Flood frequency hydrology: 3. A Bayesian analysis. Water Resour. Res. 49, 675–692.
Wilby, R.L., Harris, I., 2006. A framework for assessing uncertainties in climate change impacts: low-flow scenarios for the River Thames, UK. Water Resour. Res. 42.
Xu, Y., Gao, X., Giorgi, F., 2010. Upgrades to the reliability ensemble averaging method for producing probabilistic climate-change projections. Clim. Res. 41, 61–81.
Yan, H., Wei, W., Soon, W., An, Z., Zhou, W., Liu, Z., Wang, Y., Carter, R.M., 2015. Dynamics of the intertropical convergence zone over the western Pacific during the Little Ice Age. Nat. Geosci. 8, 315.
Zhang, Junlong, Li, Y., Huang, G., Chen, X., Bao, A., 2016a. Assessment of parameter uncertainty in hydrological model using a Markov-Chain-Monte-Carlo-based multilevel-factorial-analysis method. J. Hydrol. 538, 471–486.
Zhang, J.L., Li, Y., Huang, G., Wang, C., Cheng, G., 2016b. Evaluation of uncertainties in input data and parameters of a hydrological model using a bayesian framework: a case study of a snowmelt–precipitation-driven watershed. J. Hydrometeorol. 17, 2333–2350.
Zhang, Z., Wagener, T., Reed, P., Bhushan, R., 2008. Reducing uncertainty in predictions in ungauged basins by combining hydrologic indices regionalization and multiobjective optimization. Water Resour. Res. 44.
Zhuang, X., Li, Y., Nie, S., Fan, Y., Huang, G., 2018. Analyzing climate change impacts on water resources under uncertainty using an integrated simulation-optimization approach. J. Hydrol. 556, 523–538.